RSC Advances

PAPER

View Article Online
View Journal | View Issue

Cite this: *RSC Adv.*, 2016, **6**, 4458

Theoretical exploration of seleno and tellurophenols as promising alternatives to sulfur ligands for anchoring to gold (111) materials†

Sebastián Miranda-Rojas,*[a] Richard Salazar-Molina,*[b] Johannes Kästner,[c] Ramiro Arratia-Pérez[d] and Fernando Mendizábal[b]

Received 20th October 2015
Accepted 22nd December 2015

DOI: 10.1039/c5ra21964g

www.rsc.org/advances

It is widely known that sulfur ligands, such as alkanethiols or phenothiols and their derivatives, are useful anchor systems for gold materials due to the high affinity of sulfur to gold surfaces. In this study we use DFT calculations and a 42-atom gold cluster model to study the interaction between selenophenol and tellurophenol-derivatives with the Au(111) surface to gain information towards potential new gold-based materials. We modulated the interaction strength by controlling the charge transfer process of a particular interaction by chemically modifying the ligands. To obtain a complete analysis, we studied the ligands in their protonated, anionic and radical states aiming to cover the three possibilities in which these may interact with the gold cluster. In order to get a deeper insight into the nature of the interaction we used several analysis techniques such as energy decomposition analysis (EDA), non-covalent interactions (NCI) and natural population analysis (NPA). Our results reveal that tellurium in the anionic state provides complexes of better thermodynamic stability by ~12.0 kcal mol, when compared with the strongest sulfur–gold complex, also in the anionic state. Furthermore, this indicates that the anionic ligand is probably the dominant state for both selenium and tellurium as observed previously for sulfur. The extent to which the interaction strength could be controlled directly depends on the state of the anchor atom. In our case the anionic state is the most suitable for tuning the interaction. Finally, our main findings suggest that exchanging sulfur with selenium or tellurium involves an important increase of the interaction strength, thus, making these selenophenol and tellurophenol derivatives attractive for the development of new functional materials.

Introduction

Nowadays, the development of new technologies is expanding at an incredible rate, and as a result there is an ever increasing demand for new ideas on how to use chemistry in novel ways in order to broaden the spectrum of possibilities. An important area of research is the modification of the properties of certain materials by addition of new ligands, which are able to modify or even provide functionalities that the material itself does not possess. Some examples are the design of molecular wires for micro and nanoscale electronics,[1–3] modification of frictional and mechanical properties,[4,5] tarnish resistance,[6] molecular recognition,[7,8] catalysis,[8] and protein interaction.[9] One of the main challenges is to develop new strategies to attach these ligands to the surface. Sulfur has been widely used as an anchor atom to attach ligands to gold-based materials as for example in self-assembled monolayers (SAM), which have been shown to be useful for several applications, such as those mentioned above.[2,5,8–16]

Recently, some of us reported on a theoretical study in which we described the sulfur–gold interaction for a series of *para* substituted thiophenols in their protonated, anionic and radical states.[17] The conformation of their interaction was shown to be dependent on the ligand protonation state, where the thiophenols preferred an Au top-site conformation, while the anions and radicals adopted a bridge conformation. Our results revealed that the anionic thiophenolate formed the most stable complex showing both electrostatic and covalent contributions with charge donation to the gold material, whereas radical ligands behaved as charge acceptors. The interaction of

[a]*Chemical Processes and Catalysis (CPC), Departamento de Ciencias Químicas, Facultad de Ciencias Exactas, Universidad Andres Bello, Avenida República 275, Santiago, Chile. E-mail: sebastian.miranda@unab.cl*

[b]*Departamento de Química, Facultad de Ciencias, Universidad de Chile, P.O. Box 653, Las Palmeras 3425, Ñuñoa, Santiago, Chile*

[c]*Institut für Theoretische Chemie, Universität Stuttgart, Pfaffenwaldring 55, 70569 Stuttgart, Germany*

[d]*CENAP, Centro de Nanociencias Aplicadas, Doctorado en Fisicoquímica Molecular, Relativistic Molecular Physics (ReMoPh) Group, Universidad Andres Bello, República 275, Santiago, Chile*

† Electronic supplementary information (ESI) available: The geometric parameters of all the complexes studied in this work are listed. In addition, figure for NCI analysis of a selected radical system is deposited. See DOI: 10.1039/c5ra21964g

thiophenols with the gold surface was dominated by dispersive forces with some charge transfer to the gold cluster.

The most relevant finding was that for the anionic thiophenolate case, the interaction energy correlated with the amount of charge transferred to the gold cluster. It was possible to modulate the interaction strength by the use of electron–donor groups to increase it and electron-withdrawing groups to decrease it. However, for the thiophenols where the magnitude of charge transfer was low compared to the amount of dispersion contribution, the interaction energy was hardly modulated by the functional groups.

Sulfur belongs to the chalcogens group, elements that have six valence electrons as a common feature and belong to the group 16 in the periodic table. If we assume that the affinity of sulfur (S) to gold is determined by the electronic structure of the valence shell, we could state that all chalcogens are good candidates as anchor atoms. From this group, selenium (Se) and tellurium (Te) have more electronic density and are less electronegative than S, leading us to propose that these two atoms should act as stronger anchor atoms to gold materials than S, based on the assumption that Se and Te may be able to transfer more charge to the gold material. This is supported by our previous findings, from which we stated that the charge transfer was the dominant contribution to the S–Au interaction. In addition, experimental evidence supports the advantage of using Se in the form of diphenyl diselenides,[18–23] molecules that dissociate into selenophenolates, as activating agents for catalysis, as ligands of catalytically active metal complexes, and SAM generation.[24,25] Analogous results using diphenyl ditellurides and telluride-based chelating ligands have also been reported.[18,23,26–28] A complete experimental report on the advantage of using Se over S for SAM was recently published.[29] They compared 6-cyanonaphthalene-2-thiolate with 6-cyanonaphthalene-2-selenolate as building blocks for SAM generation, concluding a higher stability of the Se–Au bond as compared to S–Au. They also found very similar charge transfer properties for the S–Au and Se–Au bonds, measured by resonant Auger electron spectroscopy. Regarding Te, it was found that it forms the strongest interaction with Au(111) among Te, Se and S.[28] However, it seems to suffer an oxidative process resulting in less stable SAMs. Therefore, experimental data demonstrate the strong electron–donor properties of Se and Te and their usefulness towards the design of new functionalized materials.

Herein, we present a computational exploration of the interaction of a complete series of seleno- and tellurophenol ligands with a 42 atom gold cluster, which represents the (111)-surface of gold. The aim of our work is to test the hypothesis presented above, and to predict the behavior of Se and Te with gold-based materials. In addition, we present to what extent it is possible to modulate the strength of the interaction. We also provide an exhaustive characterization of the properties of the Se and Te interaction with gold materials to establish the fundamental chemical nature of this interaction.

Models and computational details

The cluster used to model the properties of the gold nanomaterial was defined as a 42 gold atom system (111) with three layers of 14 Au atoms each (Au_{42}) as depicted in Fig. 1. This cluster has proven to be a suitable model for complex interactions with gold materials and to reproduce experimental data with reasonable accuracy.[17,30–32] To explore the chemical nature of the interactions between seleno- and tellurophenol with gold materials, we used ligands with 10 different functional groups (Fig. 1) to study their behavior and to find correlations. To compare our results with the previously obtained data for the interaction of sulfur with Au_{42}, we used the same methodology.[17] There is still controversy about the final state of these types of ligands after binding to the surface, which may involve physisorption or chemisorption, depending on the protonation state and multiplicity of the chalcogen.[31,33] If it is protonated, physisorption is probably driven by dispersion forces and should be the dominant process, whereas if it is deprotonated either in its anionic or radical form, chemisorption with some covalent contribution is most probable. To assess the most probable configuration after complex formation, we considered the protonated, the anionic and radical forms of each series, having a total of 60 ligands. It should be noted that we do not aim to examine the contribution of the interaction between the functional group and the gold surface, we in fact seek to prevent that interaction. Our main interest was to assess the indirect electronic effect that the functional groups have in the interaction between the chalcogen and the gold surface. Therefore, the cluster size was defined so as to include most of the ligand–gold interaction, but preventing the involvement of the functional groups in the interaction. Despite that the aromatic ring unavoidably interacts with the gold surface and contributes to the interaction energy, this should contribute with a similar magnitude on every ligand. Thus, the increase or decrease of the interaction energies caused by the substituent effects is the only variable that defines the differences in the interaction strength, which is the main focus of this work.

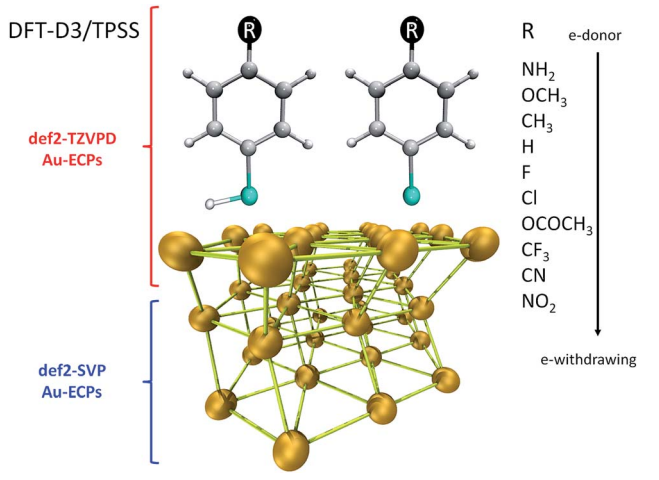

Fig. 1 Schematic representation of the molecular systems and level of theory used to model the gold–chalcogen interaction. The selenium and tellurium atoms (left: protonated, right: anionic/radical) are represented by cyan spheres. At the bottom, the gold cluster of 42 atoms is shown.

All the geometry optimizations were carried out with Turbomole v.6.5 software.[34] The gold cluster was fixed during the optimization, allowing only the ligand to freely relax above the cluster surface. This was to isolate the interaction energy between the ligand and the surface in terms of the electronic contribution between the anchor atom and the surface, avoiding introducing the contributions due to conformational changes in the surface. However, to test the effect of the surface relaxation we sampled some of the optimized complexes and re-optimized their geometries by allowing to relax the first layer of gold atoms. This resulted in an increase of the interaction energy non larger than 1.6 kcal mol^{-1}, proving that this contribution was only minor. Density functional theory in complement with the *meta*-GGA TPSS density functional,[35] was chosen as the proper level of theory as it is supported by previous works.[17,36,37] The basis set consisted of a mixed scheme described in Fig. 1, in which we used def2-TZVPD[38] for the ligand and the first layer of the cluster defined as the surface, while a def2-SVP[39] basis set was used for the two remaining Au layers. The dispersion correction by Grimme[40–42] was used to improve the accuracy of the energetic and conformational description of the complexes. Its use is indicated by using "TPSS-D3" as acronym of the density functional. Additionally, the counterpoise correction was used to eliminate the basis set superposition error (BSSE) from the interaction energies. Effective core pseudopotentials (ECPs) were used for Au, Se and Te.[43–45] The resolution of identity approach (RI)[46,47] was used to increase the efficiency of the calculations and save computational cost. Our computational scheme had been proven to be accurate enough to reproduce experimental interaction strengths between sulfur and the gold cluster,[17] thus providing a solid ground for the predictive focus of the present report. We performed a natural population analysis (NPA)[48] to get a picture of the electron transfer that is caused by complex formation.

Energy decomposition analysis (EDA) based on the Morokuma-Ziegler partitioning scheme was calculated[49] as implemented in the ADF code,[50] to obtain a clearer picture of the contributions to the Se/Te–Au interaction. This scheme considers that the interaction energy can be decomposed into an orbital and a steric contribution ($\Delta E_{int} = \Delta E_{orb} + \Delta E_{steric}$), with the orbital contribution as the dominant stabilizing factor due to its covalent character, whereas the steric interaction stands for the destabilizing part of the interaction. The latter is calculated as the sum of the electrostatic interaction (ΔE_{elstat}), which is stabilizing, and the Pauli pair repulsion (ΔE_{pauli}) as the destabilizing and main contribution to the steric interaction. The TZP/TPSS scheme was used accompanied by the two component zero-order regular approximation (ZORA)[51] hamiltonian to take the relativistic effects into account.

Finally, the analysis of the interactions of the ligands with the gold surface was extended using the NCI (Non-Covalent Interactions) index.[52,53] This analysis is able to provide a picture of the regions in real space, in which non-covalent interactions are taking place clarifying their different contributions. It can also distinguish between those regions with an attractive or repulsive component, complemented by a relative measure of the strength of these contributions. This is achieved by the generation of color-coded isosurfaces, which represent these interactions in the intermolecular space in a chemically intuitive manner.

Results and discussion

The results are presented and discussed by comparatively analyzing the complexes obtained with Se and Te in the protonated (pr), anionic (an) and radical (rad) states. We started with the inspection of their geometries (Fig. 2 and 3), followed by the analysis of the interaction energies (Tables 1–3 and Fig. 4, 6 and 8). The results were rationalized by using the EDA approach (Table 4) and the NCI index (Fig. 5 and 7), thus providing a qualitative picture of the chemical nature of the interaction. Finally, we present the analysis of the charge transfer processes and their correlation with the interaction energies according to the data listed in Tables 5 and 6.

Adsorption conformation analysis

The protonated seleno- (pr-Se) and tellurophenol (pr-Te) derivatives were adsorbed onto the gold surface adopting the Au top-site conformation. This interaction mode involves the chalcogen positioning on top of an Au atom with the interaction axis X–Au (X = Se, Te) orthogonal to the cluster surface. This is denoted by the values of θ and ω defined in Fig. 2, which are close to 90° for both pr-Se and pr-Te complexes. The interaction distance between the chalcogen and the closest gold atom from the surface was defined as D_{top} and is depicted on Fig. 2. The resulting complexes showed an average distance of 2.68 ± 0.11 and 2.77 ± 0.02 Å for pr-Se ligands and pr-Te ligands, respectively. The standard deviations show that between each subset of ligands (pr-Se and pr-Te) the variations among the

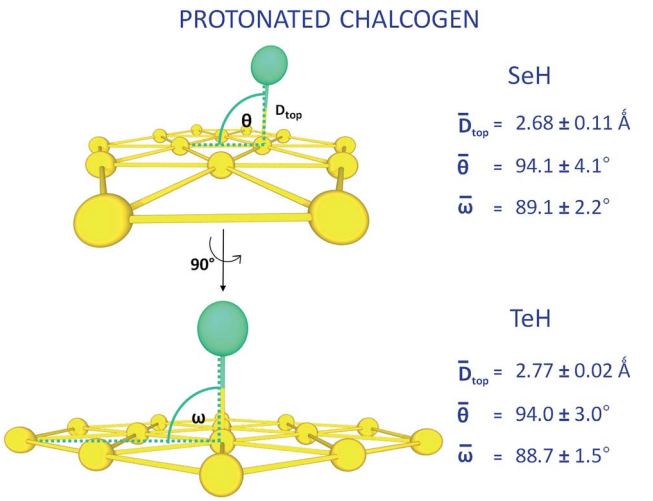

Fig. 2 Graphical representation of the main geometrical parameters obtained for the conformations of the Au_{42}–XH interaction (X = Se, Te) adopted by the seleno- and tellurophenols (protonated state). The values presented correspond to the average value calculated from the complete set of ligands with the corresponding standard deviation. The first layer of gold atoms is pictured by the yellow spheres and the chalcogen by the green sphere.

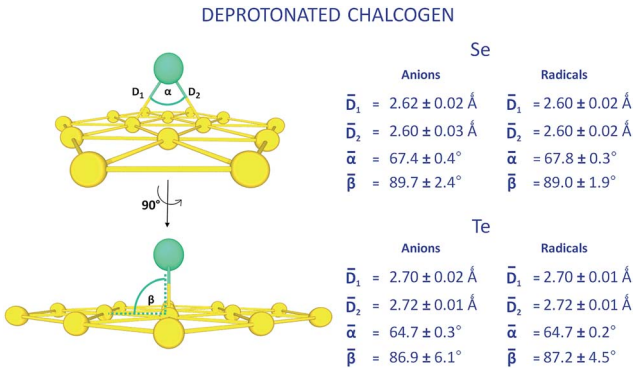

Fig. 3 Graphical representation of the main geometrical parameters obtained for the conformations of the Au_{42}–X interaction (X = Se, Te) adopted by the seleno- and tellurophenolate (anionic and radical states). The values presented correspond to the average value calculated from the complete set of ligands with the corresponding standard deviation. The first layer of gold atoms is pictured by the yellow spheres and the chalcogen by the green sphere.

Table 1 BSSE-corrected interaction energies between Au_{42} and *para* substituted seleno- and tellurophenols, pr-Se and pr-Te. The energies listed correspond to the total interaction energies ΔE_{int}(TPSS-D3) and without the dispersion contribution ΔE_{int}(TPSS). The percentage of dispersion term is included. All the energies are in kcal mol^{-1}

	ΔE_{int}(TPSS-D3)		ΔE_{int}(TPSS)		% dispersion	
Au_{42}–XH (X = Se, Te)	Se	Te	Se	Te	Se	Te
Au_{42}–$XHC_6H_4NH_2$	−44.3	−48.8	−6.6	−9.2	85.1	81.1
Au_{42}–$XHC_6H_4OCH_3$	−43.3	−47.9	−5.2	−7.7	88.0	83.9
Au_{42}–$XHC_6H_4CH_3$	−40.7	−45.6	−3.5	−6.7	91.4	85.3
Au_{42}–XHC_6H_5	−38.4	−44.4	−3.5	−7.2	90.9	83.8
Au_{42}–XHC_6H_4F	−34.2	−40.4	−2.4	−6.1	93.0	84.9
Au_{42}–XHC_6H_4Cl	−40.0	−45.8	−2.8	−6.6	93.0	85.6
Au_{42}–$XHC_6H_4OCOCH_3$	−35.0	−41.1	−1.5	−5.4	95.7	86.9
Au_{42}–$XHC_6H_4CF_3$	−34.4	−40.7	−0.5	−4.7	98.5	88.5
Au_{42}–XHC_6H_4CN	−37.9	−43.4	−1.4	−4.8	96.3	88.9
Au_{42}–$XHC_6H_4NO_2$	−37.6	−43.7	−1.7	−5.7	95.5	87.0

Table 2 BSSE-corrected interaction energies between Au_{42} and anionic *para* substituted seleno- and tellurophenolates, an-Se and an-Te. The energies listed correspond to the total interaction energies ΔE_{int}(TPSS-D3) and without the dispersion contribution ΔE_{int}(TPSS). The percentage of dispersion term is included. All the energies are in kcal mol^{-1}

	ΔE_{int}(TPSS-D3)		ΔE_{int}(TPSS)		% dispersion	
Au_{42}–X^- (X = Se, Te)	Se	Te	Se	Te	Se	Te
Au_{42}–$XC_6H_4NH_2$	−96.8	−103.7	−66.1	−70.4	31.7	32.1
Au_{42}–$XC_6H_4OCH_3$	−96.6	−103.3	−63.4	−68.0	34.4	34.2
Au_{42}–$XC_6H_4CH_3$	−94.5	−101.1	−63.2	−67.7	33.1	33.0
Au_{42}–XC_6H_5	−91.0	−98.5	−61.2	−66.6	32.7	32.4
Au_{42}–XC_6H_4F	−89.3	−96.7	−59.5	−64.7	33.4	33.1
Au_{42}–XC_6H_4Cl	−87.4	−95.1	−56.3	−61.4	35.6	35.4
Au_{42}–$XC_6H_4OCOCH_3$	−85.2	−92.9	−54.8	−60.4	35.7	35.0
Au_{42}–$XC_6H_4CF_3$	−83.5	−90.5	−52.3	−59.0	37.4	34.8
Au_{42}–XC_6H_4CN	−79.5	−87.1	−49.4	−55.2	37.9	36.6
Au_{42}–$XC_6H_4NO_2$	−75.2	−84.3	−44.2	−50.6	41.2	40.0

Table 3 BSSE-corrected interaction energies between Au_{42} and radical *para* substituted seleno- and tellurophenolates, rad-Se and rad-Te. The energies listed correspond to the total interaction energies ΔE_{int}(TPSS-D3) and without the dispersion contribution E_{int}(TPSS). The percentage of dispersion term is included. All the energies are in kcal mol^{-1}

	ΔE_{int}(TPSS-D3)		ΔE_{int}(TPSS)		% dispersion	
Au_{42}–X$^\bullet$ (X = Se, Te)	Se	Te	Se	Te	Se	Te
Au_{42}–$XC_6H_4NH_2$	−54.8	−64.8	−23.9	−31.6	56.4	51.2
Au_{42}–$XC_6H_4OCH_3$	−64.6	−70.4	−31.3	−37.3	51.5	47.0
Au_{42}–$XC_6H_4CH_3$	−63.8	−71.8	−32.6	−38.0	48.9	47.1
Au_{42}–XC_6H_5	−61.2	−69.7	−31.1	−37.4	35.2	46.3
Au_{42}–XC_6H_4F	−61.1	−69.6	−30.9	−37.3	49.4	46.7
Au_{42}–XC_6H_4Cl	−61.5	−70.1	−29.9	−36.2	51.4	48.4
Au_{42}–$XC_6H_4OCOCH_3$	−55.4	−69.4	−24.5	−36.4	55.8	47.6
Au_{42}–$XC_6H_4CF_3$	−60.5	−68.8	−28.7	−34.6	52.6	49.7
Au_{42}–XC_6H_4CN	−60.6	−68.7	−29.8	−35.5	50.8	48.3
Au_{42}–$XC_6H_4NO_2$	−59.8	−66.4	−27.7	−31.0	53.7	53.3

interaction distances were only minor. This exposes that the functional group does not affect the binding conformation. The increase in interaction distance observed for the pr-Te compared to the pr-Se complexes was only marginal (0.09 Å). The change in the C–X bond distance (Tables S1 and S2†) was larger, 1.92 ± 0.03 Å for pr-Se and 2.12 ± 0.01 Å for pr-Te, and almost unaffected by the substituent. This 0.20 Å difference is close to the vdW radius difference between Se and Te (1.90 and 2.06 Å, respectively). The list of geometric parameters for pr-X–Au_{42} (X = Se, Te) complexes can be found in Tables S1 and S2 of the ESI.†

The adsorption of the anionic ligands (an-Se and an-Te) on the gold surface involved the interaction of the anchor atom with two Au atoms. The chalcogen was positioned above the Au–Au bond, as pointed out by the β parameter defined in Fig. 3, adopting what is commonly defined as a bridge conformation. Similar to the protonated ligands, the interaction geometry of the complexes were insensitive to the type of substituent, denoted by the minor variations observed in the X–Au (X = Se, Te) interaction distances defined in Fig. 3 as D_1 and D_2. The complete list of geometric parameters for the an-X–Au_{42} (X = Se, Te) complexes are presented in Tables S3 and S4 of the ESI.† The exchange of an-Se to an-Te lead to an increase in the interaction distance close to 0.10 Å in almost every case. Consequently, the Se atom from the ligands was closer to the surface than for the Te ligands probably due to its smaller size, also evident from the larger angle formed by Au–X–Au, here defined as α. The deprotonation of the chalcogen caused an increase by 0.05 Å in the average C–X bond distance, where C–Se increased from 1.92 Å to 1.97 Å and C–Te from 2.12 Å to 2.17 Å, without showing a significant variation.

The radical ligands (rad-Se and rad-Te) showed very similar conformations and interaction distances (D_1 and D_2) as the

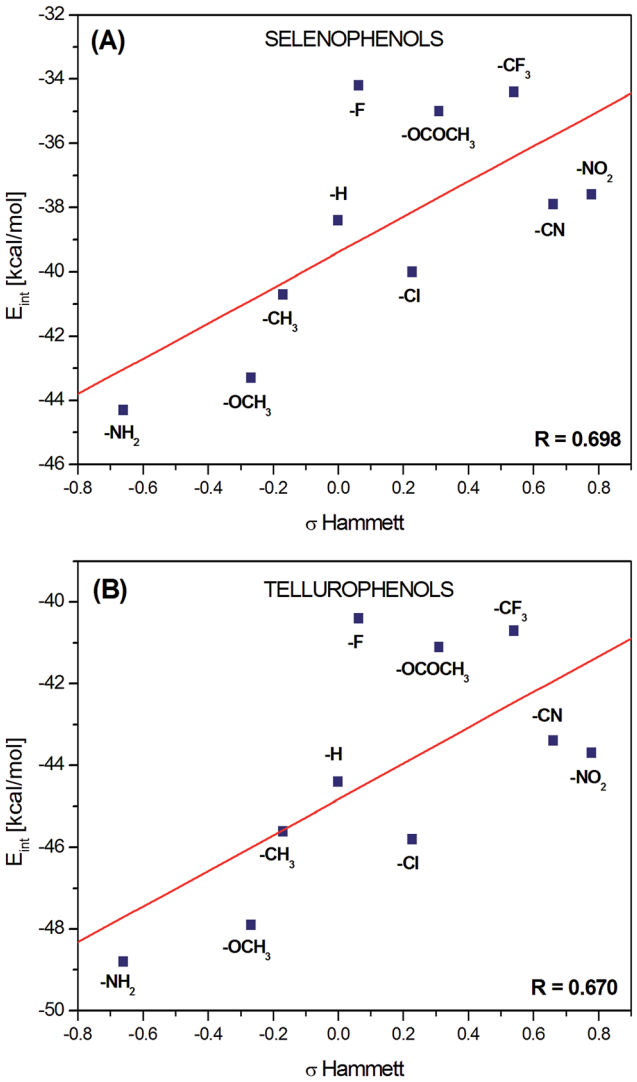

Fig. 4 Plot of the interaction energies of the selenophenol (pr-Se, (A)) and the tellurophenol series (pr-Te, (B)) *versus* the σ_{para} Hammett.

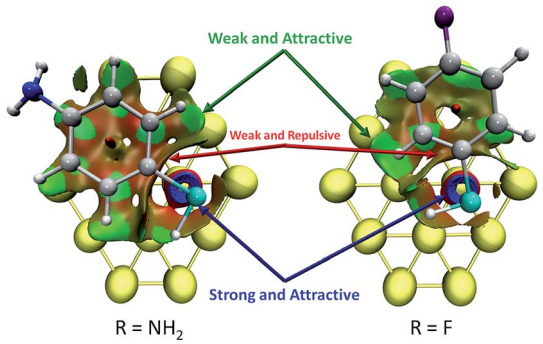

Fig. 5 Graphical representation of the non-covalent interactions between the protonated ligands, pr-Se (carbon-grey, nitrogen-blue, hydrogen-white, selenium-cyan spheres) and the gold surface (yellow spheres). At the left side there is the ligand with the strongest interaction strength ($-NH_2$) and at the right side of the picture the ligand with the weakest (–F).

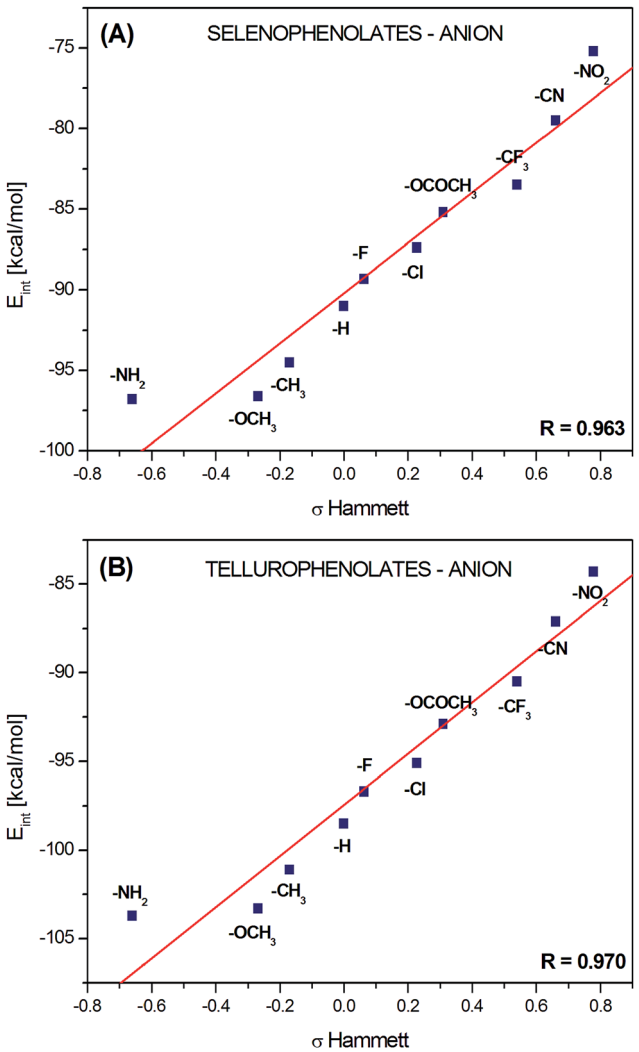

Fig. 6 Plot of the interaction energies of the anionic selenophenolate (an-Se, (A)) and tellurophenolate series (an-Te, (B)) *versus* the σ_{para} Hammett.

anionic ligands (an-Se and an-Te). As pointed out by α parameter, Se was also closer to the surface, while β showed the same behavior for Se and Te in the anionic and the radical states. The C–X bond distance was also similar to that of the anionic ligands, indicative that the slight elongation of the bond is caused just by the deprotonation, independent of the electronic state of the chalcogen atom, radical or anionic. The list of geometric parameters for the rad-X–Au_{42} (X = Se, Te) complexes can be found in Tables S5 and S6 of the ESI.†

To understand from a chemical point of view why the protonated form of the chalcogens adopt the Au top-site conformation, and the anionic together with the radicals the bridge conformation, we performed an analysis of the NAOs. After identifying the NAOs that suffered changes in their occupation number it was possible to interpret that when the chalcogen is protonated, the only NAO available as a donor is the p_z, whereas the d_{z^2} orbital from one Au atom from the surface acts as the main charge acceptor. This leads the anchor atom to

Table 4 Energy decomposition analysis. The data is presented according to the average values obtained from each set of ligands

Model system	% orb	% elect	Steric (kcal mol^{-1})
Au_{42}–SeH	43.1	56.9	22.2
Au_{42}–TeH	40.8	59.2	26.9
Au_{42}–Se^-	38.0	62.0	49.1
Au_{42}–Te^-	35.7	64.3	59.6

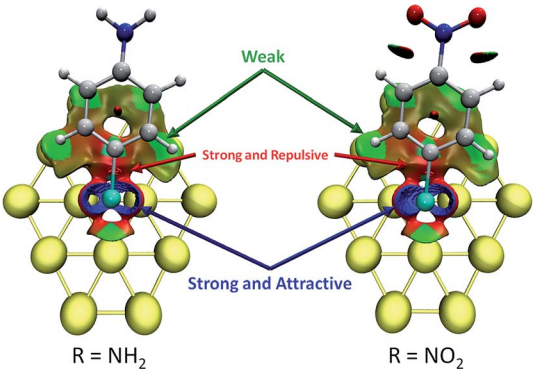

Fig. 7 Graphical representation of the non-covalent interactions between the anionic ligands, an-Se (carbon-grey, nitrogen-blue, hydrogen-white, selenium-cyan spheres) and the gold surface (yellow spheres). At the left side there is the ligand with the strongest interaction strength (–NH_2) and at the right side of the picture the ligand with the weakest (–NO_2).

position itself on top of one of the gold atoms where the d_{z^2} orbital is localized. Meanwhile, the deprotonation of the chalcogen makes an extra p_y orbital available as a charge donor (or acceptor in the case of the radicals). Due to the spatial configuration of p_y and p_z, these two orbitals are able to interact with a combination of the d_{z^2} and d_{yz} orbitals from two gold atoms as revealed by the NAO analysis, which correspond to the orbitals from the gold cluster involved in the interaction. It should be noted that the charge delocalization on gold material seems to be more complex and involves more orbitals than the reduced picture provided by our analysis, even though the description provided by our results is enough to get a qualitative explanation of the binding conformations.

$Au_{42}\cdots$XH interaction strength (X = Se, Te/protonated state)

The interaction energies for pr-Se and pr-Te are listed in Table 1. The energies obtained for pr-Se ligands range between −34.2 and −44.3 kcal mol^{-1} for R = F and R = NH_2, respectively (where R stands for the *para*-substituent as depicted in Fig. 1). The variation between the lowest and the highest interaction energy was of 10.1 kcal mol^{-1}. This small variation denotes the rather low influence of the substituent group on the interaction with the gold cluster. The interaction energies without the dispersion contribution averaged to a value of −2.9 kcal mol^{-1}. Consequently, the dispersion contribution was very high with

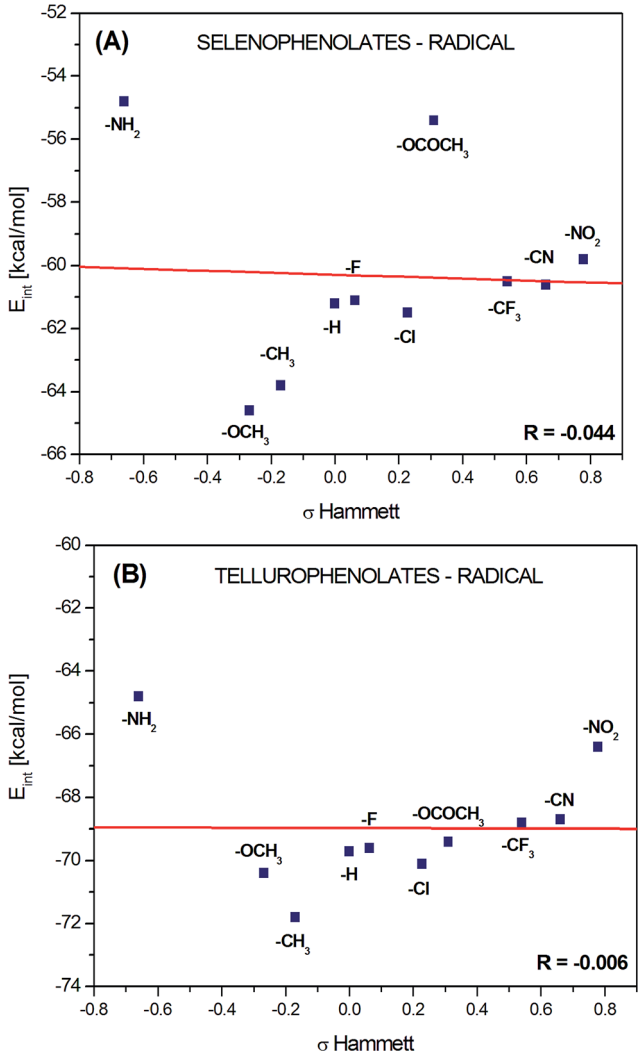

Fig. 8 Plot of the interaction energies of the radical selenophenolate (rad-Se, (A)) and tellurophenolate series (rad-Te, (B)) *versus* the σ_{para} Hammett.

a maximum of 98.5% of the total interaction energy for the case of R = CF_3 and an average of 92.7%.

The interaction energies calculated for the pr-Te ligands range between −40.8 and −48.8 kcal mol^{-1} for R = F and R = NH_2, respectively; following the same behavior as the pr-Se ligands. The variation of the interaction energies for the pr-Te ligands was 8.4 kcal mol^{-1}, slightly lower than the obtained for the pr-Se ligands (10.1 kcal mol^{-1}). However, the interaction energies of pr-Te ligands without the dispersion contribution were more than twice the magnitude observed for the pr-Se ligands, with an average value of −6.4 kcal mol^{-1}, indicative of a higher covalent and electrostatic contribution of the pr-Te than pr-Se. The magnitude of the dispersion contribution was similar between both anchor atoms, with average values of −35.7 and −37.8 kcal mol^{-1} for pr-Se and pr-Te, respectively.

Regarding the interaction between the chalcogen and the gold surface, both pr-Se and pr-Te sets of ligands showed a similar behavior, as depicted in Fig. 4; in which the interaction

Table 5 Quantification of the charge transfer process obtained from the difference between the NPA charges of the selenium complexes and the free fragments

	pr-Se		an-Se		rad-Se	
Substituent	Au_{42}	ΔSeH^a	Au_{42}	ΔSe^a	Au_{42}	ΔSe^a
$-NH_2$	−0.16	0.18	−0.67	0.45	0.26	−0.12
$-OCH_3$	−0.13	0.13	−0.65	0.43	0.28	−0.16
$-CH_3$	−0.12	0.13	−0.64	0.42	0.29	−0.19
–H	−0.12	0.12	−0.63	0.41	0.30	−0.21
–F	−0.12	0.12	−0.63	0.41	0.31	−0.20
–Cl	−0.13	0.12	−0.61	0.38	0.32	−0.21
$-OCOCH_3$	−0.11	0.12	−0.60	0.37	0.32	−0.21
$-CF_3$	−0.11	0.11	−0.59	0.32	0.34	−0.24
–CN	−0.11	0.10	−0.57	0.30	0.36	−0.24
$-NO_2$	−0.07	0.10	−0.53	0.22	0.38	−0.26

[a] Values represent the amount of charge donated directly by the chalcogen atom and it was obtained from the difference between the chalcogen charge in the complex and the free ligand.

Table 6 Quantification of the charge transfer process obtained from the difference between the NPA charges of the tellurium complexes and the free fragments

	pr-Te		an-Te		rad-Te	
Substituent	Au_{42}	ΔTeH^a	Au_{42}	ΔTe^a	Au_{42}	ΔTe^a
$-NH_2$	−0.22	0.26	−0.83	0.66	0.10	0.02
$-OCH_3$	−0.20	0.21	−0.81	0.65	0.15	−0.02
$-CH_3$	−0.19	0.20	−0.80	0.63	0.14	−0.05
–H	−0.18	0.20	−0.79	0.62	0.15	−0.06
–F	−0.19	0.20	−0.79	0.63	0.15	−0.06
–Cl	−0.17	0.20	−0.77	0.60	0.16	−0.07
$-OCOCH_3$	−0.17	0.18	−0.76	0.59	0.17	−0.07
$-CF_3$	−0.17	0.17	−0.76	0.55	0.19	−0.11
–CN	−0.13	0.17	−0.73	0.51	0.18	−0.11
$-NO_2$	−0.08	0.16	−0.71	0.42	0.22	−0.13

[a] Values represent the amount of charge donated directly by the chalcogen atom and it was obtained from the difference between the chalcogen charge in the complex and the free ligand.

energies are plotted against the σ Hammett of the functional groups. Among the electron-withdrawing groups, R = Cl showed the highest interaction energy in opposition to R = F, which according to its σ-Hammet was expected to have a higher interaction strength than R = Cl. On the other hand, the ligands with R = NO_2 and R = CN, which were expected to have the lowest interaction energies of the series because of their high electron-withdrawing power, showed higher values than R = F, R = $OCOCH_3$ and R = CF_3. Consequently, there was no linear correlation between the electron donating or withdrawing properties of the functional groups and the total interaction energy. This is also denoted by the correlation factor (R) of 0.698 and 0.670 for pr-Se and pr-Te, respectively. The obtained results pointed out the difficulty to modulate the strength of the interaction between the protonated ligands and gold materials by means of controlling the charge transfer process.

The results from the NCI analysis are shown in Fig. 5, where the pr-Se ligands with the strongest and the weakest interaction strengths are shown (R = NH_2 and R = F, respectively). Se was chosen for this analysis because it represents an intermediate species between S and Te. According to the NCI approach, the most attractive contribution is located between the anchor atom and the gold atom identified as the dominant non-covalent contribution. Then, it follows the weak but stabilizing interactions denoted by the regions colored in green. These are located in the regions where the atoms from the aromatic ring are above of a gold atom from the surface, probably involving the polarization of atom centered orbitals from the ligand and the cluster. Interestingly, the regions in which the ligand is located above of the bonding area of the gold cluster result in weak but repulsive interactions (see Fig. 5).

$Au_{42}\cdots X$ interaction strength (X = Se, Te/anionic state)

The complete list of interaction energies for an-Se and an-Te is presented in Table 2. The an-Se ligands show increased interaction energies compared to the neutral state, ranging from 10.1 to 21.6 kcal mol^{-1}, with energies from −75.2 kcal mol^{-1} for R = NO_2 to −96.8 kcal mol^{-1} for R = NH_2, thus pointing out the influence of the substituent effect in this type of interaction. The average interaction energy without the dispersion contribution was of −57.0 kcal mol^{-1}, an increase that allows us to infer the participation of covalent and electrostatic components into the interaction. Meanwhile, the dispersion contribution averaged to −30.9 kcal mol^{-1}, with a decrease of 4.8 kcal mol^{-1} compared to the protonated state. Despite that, the dispersion contribution is similar to that obtained for the protonated ligands, the bonding contribution is higher, thus significantly decreasing its average contribution to the total interaction energy from 92.7% (protonated) to 35.3% (anionic).

The interaction strength of the an-Te ligands varied between −84.3 and −103.7 kcal mol^{-1} for R = NO_2 and R = NH_2, respectively; with a range of 19.4 kcal mol^{-1}, very similar to the one obtained for the an-Se counterpart (21.6 kcal mol^{-1}). Furthermore, there is an increase in their strength compared to the an-Se ligands, showing the highest interaction energies obtained in the present work, also exposing the stability of these complexes when compared with the rest of the series. The average interaction energy without the dispersion contribution was −62.4 kcal mol^{-1}, a value that denotes the dominant covalent and electrostatic character of the interaction as stated for an-Se ligands. The ligand with the largest increase of interaction strength, due to the change of anchor atom from Se to Te was the one with R = NO_2 as functional group, which increased by 9.1 kcal mol^{-1}. In terms of percentage, the dispersion contribution was almost the same between both anchor atoms in their anionic states, with values of 35.3% and 34.7% for an-Se and an-Te, respectively.

The deprotonation of pr-Se and pr-Te led to a strong increase in the interaction strength. In order to quantify this increase, we compared the averaged values of the interaction energies of the complete sets of protonated and anionic ligands, revealing an

increase of 49.3 kcal mol^{-1} after the deprotonation of pr-Se, and of 51.1 kcal mol^{-1} for pr-Te.

As previously obtained with S as the anchor atom,[17] the anionic ligands with Se and Te showed a linear correlation between the interaction energies and the σ-Hammett of their *para*-substituents as shown in Fig. 6, with *R* of 0.963 and 0.970 for Se and Te, respectively. This reveals that the interaction strength for the an-Se and an-Te ligands can be modulated through chemical modifications of the ligands in a similar fashion as the sulfur ligands. The only substituent that does not behave as expected is R = NH_2, which should have a higher interaction strength instead of a value very similar to the ligand with R = OCH_3. This may be related to the limited capacity of the gold cluster to receive charge, which probably is reaching the limit with R = OCH_3. This problem should not be faced when working with the real material, which will act as a limitless deposit of electronic density.

The NCI analysis is presented in Fig. 7, where the Se ligands with the strongest and the weakest interaction strengths are shown (R = NH_2 and R = NO_2, respectively); following the same criteria used for the protonated ligands. The resulting diagrams expose the strong and attractive interaction between the anchor atom and the region comprehended between the two gold atoms with which it interacts. This is an interesting feature, as the anchor atom is able to interact with the bonding region between two gold atoms, whereas the rest of the atoms from the ligand involve only repulsive interactions in regions of similar properties. On the other hand, it seems that as a result of the closer interaction between the chalcogen and the gold surface, the carbon bonded to the chalcogen is also closer to the surface, corresponding to a bonding region of the cluster. As such, it results in a repulsive interaction, stronger than the observed for the protonated ligands. From the non-covalent contributions, it does not seem to be a noticeable difference between R = NH_2 and R = NO_2, pointing out that the main difference is in the covalent part of the interaction.

$Au_{42}\cdots X^{\cdot}$ interaction strength (X = Se, Te/radical state)

The results associated to the interaction energies of the radical ligands (rad-Se and rad-Te) are listed in Table 3. The interaction energies of the rad-Se ligands in the radical state occupy an intermediate place regarding the other two states of the anchor atom, varying between −54.8 and −64.6 kcal mol^{-1} for R = NH_2 and R = OCH_3, respectively; both ligands with electron–donor groups. This gives a spread of 9.8 kcal mol^{-1}, which is close to the one obtained for the protonated ligands (10.1 kcal mol^{-1}). Despite of this, the rest of the ligands showed just minor variations in their interaction energies showing an almost invariant behavior as depicted in Fig. 8. Thus, the electronic effect of the different substituents almost vanishes when the ligand is in the radical state.

The averaged interaction energies without dispersion contribution showed a value of −29.0 kcal mol^{-1}, similar to the magnitude obtained for the average of the dispersion contribution that resulted in −31.3 kcal mol^{-1}. This denotes that dispersion has a similar weight on the interaction energy as the covalent and electrostatic contributions for these complexes. This is shown by the average weight of the dispersion forces of 52.0% with respect to the total interaction energy.

The rad-Te ligands showed higher interaction energies, consistent with the trend from the analysis of the protonated and anionic ligands. In this case the highest interaction energy corresponded to R = CH_3 with −71.8 kcal mol^{-1}, followed by R = OCH_3 with −70.4 kcal mol^{-1}. The lowest interaction energy was for R = NH_2, as observed for the rad-Se series, with a value of −64.8 kcal mol^{-1}. The range over the complete series of rad-Te was of 7.0 kcal mol^{-1} showing the low influence of the substituents on the interaction energy. The averaged interaction energy without dispersion was −35.5 kcal mol^{-1}, pointing out that the dispersion contribution was of the same order as observed for rad-Se, with an average value of 52.0%, close to the half of the interaction energy. As discussed above for the rad-Se ligands, here there is also almost no effect of the substituent group, thus reinforcing the idea of a lack of influence from the substituent group to the strength of the interaction with gold materials. The only common behavior was observed for R = NH_2, which showed the lowest interaction energy with both anchor atoms.

Determination of the NCI resulted in similar features to those observed for the anionic ligands, results shown in Fig. S1.† This denotes just a minor role of the electronic state of the anchor atom in the non-covalent interactions. The only minor difference comes from the fact that the region below the C–X bond and particularly the carbon features a more repulsive interaction than the one observed for the anionic ligands. This is probably a consequence of the electronic repulsion of the surface electrons and the charge accepted by the ligand.

Energy decomposition analysis (EDA)

As discussed above, the low values for the interaction energy of the protonated ligands after neglecting the dispersion term in both series of pr-Se and pr-Te ligands show the low covalent and electrostatic character of this interaction. The data obtained from the EDA analysis listed in Table 4, reveals that the covalent and electrostatic contributions to the interaction are similar, with a moderately higher contribution from the electrostatic part. The average weights for the orbital contributions were of 43.1% and 40.8% for pr-Se and pr-Te, respectively; while the electrostatic part of the interaction contributed with 56.9% and 59.2% for pr-Se and pr-Te ligands, respectively. Apparently, the ligands with pr-Te have a slightly higher electrostatic contribution compared to the orbital part. The destabilizing part of the bonding denoted by the steric interaction was 4.7 kcal mol^{-1} higher for pr-Te than pr-Se, mostly associated with the larger size of the electronic density belonging to the Te atom.

The contributions to the bonding part of the interaction determined by the EDA approach for the anionic ligands shows a slight increase of the electrostatic contribution with respect to the protonated ligands. The average weights for the electrostatic part were of 62.0% and 64.3% for an-Se and an-Te ligands, respectively. Meanwhile, the orbital contributions were 38.0% and 35.7% for an-Se and an-Te, respectively; denoting again that

an-Te has a slightly higher contribution from the electrostatic part, similar to what is observed with the protonated ligands. The increase in the steric contribution by more than a factor of two from the protonated to the anionic systems is caused by the closer interaction between the ligands and the gold surface in the anionic case. Among the anionic ligands, an-Te has the highest steric interaction despite the longer interaction distance when compared to an-Se, probably because of the larger electronic density associated to Te.

Charge transfer analysis

The idea behind the use of electron-donating and -withdrawing groups is to modulate the amount of charge transfer involved in the interaction, under the assumption that this is a determinant feature on the final interaction strength. As can be seen from the data listed in Tables 5 and 6, for both Se and Te in the protonated and anionic states, electronic density is donated towards the gold cluster whereas for the radicals the electronic density is transferred from the cluster to the ligand. Despite that the interaction of the protonated ligands are mostly a consequence of the dispersion forces, they show a component of charge transfer that correlates with the properties of the functional group responsible of the bonding contribution (see Table 5). However, the bonding contribution associated to this charge transfer corresponds to less than 20% of the total interaction energy (see Table 1), thus making it very difficult to modulate the interaction strength of the protonated ligands by the approach here proposed. The pr-Te ligands achieved to donate slightly larger amounts of charge to the cluster than pr-Se ligands, with exception of the R = NO_2 ligand, which donates almost the same amount of charge independent of the anchor atom.

With respect to the anionic systems, there is a clear correlation between the electron-donating or withdrawing properties of the substituent with the amount of charge transferred to the gold cluster, which at the same time correlates with the interaction energy. These observations support the suggestion of an interaction dominated by the bonding contributions, which according to the present results has a donor–acceptor nature. Thus, the interaction of the anionic ligands is predominantly driven by the charge transfer process, which is highly increased by the deprotonation of the ligands.

The amount of charge transferred to the gold material by the an-Te ligands is very close to a whole electron, especially for the R = NH_2 ligand. This exposes the great potential of an-Te ligands as charge donors, which explains the higher interaction energies obtained when using this anchor atom with respect to Se and S. Nevertheless, this is probably the reason of its high reactivity towards oxidation that finally leads to unstable SAMs, and this is at present the main drawback in the use of Te ligands. To assess this issue, one could test the effect of different functional groups in *meta*-position from the aromatic ring, to partially protect the Te atom towards oxidation, but without greatly affecting its interaction with the gold surface. The modification of the anchor atom from an-Se to an-Te involves an increase of the amount of charge donated to the material of *c.a.* 0.16*e*, which is almost constant along the whole series of anionic ligands, attributing this charge only to the anchor atom.

As stated above, the radical ligands act as charge acceptors, where the rad-Se ligands are able to receive more charge than rad-Te based ligands mainly due to their larger electronegativity. Despite of this, the interaction energies were moderately higher for the rad-Te than rad-Se, revealing that the nature of the radical interaction with gold-based surfaces is dominated by other effects than charge transfer. The amount of charge received by the ligand correlates with the properties of the *para*-substituent.

Comparative analysis of the interaction strength: S *versus* Se and Te

The dominant role of dispersion forces in the interaction of pr-Se and pr-Te was also observed for pr-S ligands, and consequently these also showed the lowest interaction strength compared to anionic or radical counterparts. In general, the dispersion forces ranged between 80 and 90% of the total interaction energy, although in some cases the pr-Se ligands showed contributions even higher than 90%. For the three protonated chalcogens (pr-X), the ligand with the strongest interaction energy was the one with R = NH_2 as substituent, exposing that only this electron–donor group was capable to moderately affect the stability of the complex. The highest interaction energy was obtained by using Te as the anchor atom, which was 10.3 kcal mol^{-1} higher than the one obtained for its counterpart with S, while with Se it was 5.8 kcal mol^{-1} higher than S.

The anionic state of the chalcogens provided the strongest interaction with the gold surface, where the use of Te over S lead to an increase of ~12.0 kcal mol^{-1} when using R = NH_2 as the reference ligand. Thus, Te provided the most stable complexes among the three chalcogens. One of the main reasons of this high interaction energy achieved by Te is that it is dominated by the charge transfer process, where according to our analysis Te was able to transfer larger amounts of charge to the gold cluster than S and Se.

The use of electron–donor and withdrawing substituent groups allowed to modulate the interaction energy within a range of ~20.0 kcal mol^{-1} for each chalcogen in their anionic states, thus showing a similar behavior in terms of the modulation of the interaction strength. The dispersion forces contributed in a similar manner for S, Se and Te with contributions between 30 and 40% to the interaction energy.

The radical ligands showed a moderately larger increase when replacing S with Te, than observed for the anionic ligands, with an increase of 14.3 kcal mol^{-1}. Despite of that, the total interaction energies were not as high as with the anionic ligands, where S showed a maximum value of 50.5 kcal mol^{-1} *versus* the 64.8 kcal mol^{-1} obtained with Te. In general, S, Se and Te in the radical state showed a contribution of the dispersion forces between 50 and 55%, *i.e.* close to the half of the interaction strength. As discussed above, the radicals showed an opposite behavior in terms of the nature of the X–Au

bond, in which the ligand acted as a charge acceptor instead of a donor as observed for the protonated and anionic states. If we consider the electronegativity of each chalcogen as a dominating variable in the charge transfer process, one would expect S to show the highest interaction energy among the three chalcogens, however it is Te. This reveals that there are other variables that dominate the interaction between the radical chalcogens and gold materials that may be further explored.

In summary, both selenium and tellurium ligands are predicted to be better candidates as anchor atoms to gold-based materials than sulfur ligands, where the anionic state seems to be the most probable after complex formation. This is highly advantageous as the interaction strength of these ligands is easily modulated by simple chemical modifications that at some extent are able to regulate the amount of charge transferred to the material.

Conclusions

We presented a detailed exploration of the interaction between Se and Te with gold-based materials, together with the characterization of the different chemical properties that dominate its strength. The main findings presented in this study predict that these atoms should be able to form stronger interactions with gold-based materials than the ones obtained by using sulfur-based ligands. The new insights provided by this work could be useful in the design and control of the behavior associated to these complexes. This may also lead to the generation of new systems of unexplored physicochemical properties.

As a final remark, we suggest the use of Se and Te as new anchoring atoms to gold-based materials, opening the possibility for experimentalists to explore these ligands as an innovative strategy to develop and study new functional materials.

Acknowledgements

The authors thank financial support from FONDECYT through projects No. 3130383, 1140503, and 1150629. S. M. R. thanks financial support from Grant ICM No. 120082. The authors thank to Dr Paulina Sierra-Rosales and Laura Nunes dos Santos Comprido for their careful revision of the manuscript. F. M. E and R. A. P thank to Millennium Nucleus RC120001. R. S. M. acknowledges CONICYT for his PhD scholarship No. 21130874. J. K. was financially supported by the German Research Foundation (DFG) within the Cluster of Excellence in Simulation Technology (EXC 310/2) at the University of Stuttgart.

References

1 L. Venkataraman, J. E. Klare, I. W. Tam, C. Nuckolls, M. S. Hybertsen and M. L. Steigerwald, *Nano Lett.*, 2006, **6**, 458–462.
2 D. Adams, L. Brus, C. Chidsey, S. Creager, C. Creutz, C. Kagan, P. Kamat, M. Lieberman, S. Lindsay, R. Marcus, R. Metzger, M. Michel-Beyerle, J. Miller, M. Newton, D. Rolison, O. Sankey, K. Schanze, J. Yardley and X. Zhu, *J. Phys. Chem. B*, 2003, **107**, 6668–6697.
3 C. M. Whelan, M. Kinsella, L. Carbonell, H. Meng Ho and K. Maex, *Microelectron. Eng.*, 2003, **70**, 551–557.
4 X. Xiao, J. Hu, D. H. Charych and M. Salmeron, *Langmuir*, 1996, **12**, 235–237.
5 J. E. Houston and H. I. Kim, *Acc. Chem. Res.*, 2002, **35**, 547–553.
6 T. D. Burleigh, Y. Gu, G. Donahey, M. Vida and D. H. Waldeck, *Corrosion*, 2001, **57**, 1066–1074.
7 U. Drechsler, B. Erdogan and V. M. Rotello, *Chem.–Eur. J.*, 2004, **10**, 5570–5579.
8 M. C. Daniel and D. Astruc, *Chem. Rev.*, 2004, **104**, 293–346.
9 M. Mrksich and G. M. Whitesides, *Annu. Rev. Biophys. Biomol. Struct.*, 1996, **25**, 55–78.
10 J. C. Love, L. a. Estroff, J. K. Kriebel, R. G. Nuzzo and G. M. Whitesides, *Chem. Rev.*, 2005, **105**, 1103–1169.
11 L. Dubois and R. Nuzzo, *Annu. Rev. Phys. Chem.*, 1992, **43**, 437–463.
12 P. Laibinis and G. Whitesides, *J. Am. Chem. Soc.*, 1991, **113**, 7152–7167.
13 I. Wenzl, C. M. Yam, D. Barriet and T. R. Lee, *Langmuir*, 2003, **19**, 10217–10224.
14 N. J. Brewer, B. D. Beake and G. J. Leggett, *Langmuir*, 2001, **17**, 1970–1974.
15 Y. Wang, Y. Zhou, J. Sokolov, B. Rigas, K. Levon and M. Rafailovich, *Biosens. Bioelectron.*, 2008, **24**, 162–166.
16 H. Chen, C. K. Heng, P. D. Puiu, X. D. Zhou, A. C. Lee, T. M. Lim and S. N. Tan, *Anal. Chim. Acta*, 2005, **554**, 52–59.
17 S. Miranda-Rojas, A. Munoz-Castro, R. Arratia-Perez and F. Mendizabal, *Phys. Chem. Chem. Phys.*, 2013, **15**, 20363–20370.
18 M. Wang, K. Ren and L. Wang, *Adv. Synth. Catal.*, 2009, **351**, 1586–1594.
19 D. Liotta, U. Sunay, H. Santiesteban and W. Markiewicz, *J. Org. Chem.*, 1981, **46**, 2605–2610.
20 J. Trenner, C. Depken, T. Weber and A. Breder, *Angew. Chem., Int. Ed.*, 2013, **52**, 8952–8956.
21 F. V. Singh and T. Wirth, *Org. Lett.*, 2011, **13**, 6504–6507.
22 L. Yu, H. Li, X. Zhang, J. Ye, J. Liu, Q. Xu and M. Lautens, *Org. Lett.*, 2014, **2**, 2–5.
23 C. D. Prasad, S. J. Balkrishna, A. Kumar, B. S. Bhakuni, K. Shrimali, S. Biswas and S. Kumar, *J. Org. Chem.*, 2013, **78**, 1434–1443.
24 Q. Yao, E. P. Kinney and C. Zheng, 2004, 2000–2002.
25 A. Shaporenko, P. Cyganik, M. Buck, A. Terfort and M. Zharnikov, *J. Phys. Chem. B*, 2005, **109**, 13630–13638.
26 Y. Nakayama, K. Watanabe, N. Ueyama, A. Nakamura, A. Harada and J. Okuda, *Organometallics*, 2000, **19**, 2498–2503.
27 Y. Takashima, Y. Nakayama, K. Watanabe, T. Itono, N. Ueyama, A. Nakamura, H. Yasuda, A. Harada and J. Okuda, *Macromolecules*, 2002, **35**, 7538–7544.
28 T. Weidner, A. Shaporenko, J. Mu, M. Ho, A. Terfort and M. Zharnikov, *J. Phys. Chem. C*, 2007, 11627–11635.
29 J. Ossowski, T. Wächter, L. Silies, M. Kind, A. Noworolska, F. Blobner, D. Gnatek, J. Rysz, M. Bolte, P. Feulner, A. Terfort, P. Cyganik and M. Zharnikov, *ACS Nano*, 2015, **9**, 4508–4526.

30 C. Vericat, M. E. Vela, G. Benitez, P. Carro and R. C. Salvarezza, *Chem. Soc. Rev.*, 2010, **39**, 1805–1834.
31 H. Hakkinen, *Nat. Chem.*, 2012, **4**, 443–455.
32 E. Pensa, E. Cortés, G. Corthey, P. Carro, C. Vericat, M. H. Fonticelli, G. Benítez, A. a. Rubert and R. C. Salvarezza, *Acc. Chem. Res.*, 2012, **45**, 1183–1192.
33 N. Jayanthi, J. Cruz and T. Pandiyan, *Chem. Phys. Lett.*, 2008, **455**, 64–71.
34 R. Ahlrichs, M. Bär, M. Häser, H. Horn and C. Kölmel, *Chem. Phys. Lett.*, 1989, **162**, 165–169.
35 J. Tao, J. Perdew, V. Staroverov and G. Scuseria, *Phys. Rev. Lett.*, 2003, **91**, 146401.
36 M. P. Johansson, A. Lechtken, D. Schooss, M. M. Kappes and F. Furche, *Phys. Rev. A: At., Mol., Opt. Phys.*, 2008, **77**, 53202.
37 S. Goel, K. A. Velizhanin, A. Piryatinski, S. Tretiak and S. A. Ivanov, *J. Phys. Chem. Lett.*, 2010, **1**, 927–931.
38 D. Rappoport and F. Furche, *J. Chem. Phys.*, 2010, **133**, 134105.
39 A. Schäfer, H. Horn and R. Ahlrichs, *J. Chem. Phys.*, 1992, **97**, 2571.
40 S. Grimme, J. Antony, S. Ehrlich and H. Krieg, *J. Chem. Phys.*, 2010, **132**, 154104.
41 W. Hujo and S. Grimme, *J. Chem. Theory Comput.*, 2011, **7**, 3866–3871.
42 S. Grimme, *ChemPhysChem*, 2012, **13**, 1407–1409.
43 D. Andrae, U. Häußermann, M. Dolg, H. Stoll and H. Preuß, *Theor. Chim. Acta*, 1990, **77**, 123–141.
44 G. Igel-Mann, H. Stoll and H. Preuss, *Mol. Phys.*, 1988, **65**, 1321–1328.
45 A. Bergner, M. Dolg, W. Küchle, H. Stoll and H. Preuß, *Mol. Phys.*, 1993, **80**, 1431–1441.
46 K. Eichkorn, O. Treutler, H. Oehm, M. Häser and R. Ahlrichs, *Chem. Phys. Lett.*, 1995, **242**, 652–660.
47 F. Weigend, *Phys. Chem. Chem. Phys.*, 2006, **8**, 1057–1065.
48 A. E. Reed, R. B. Weinstock and F. Weinhold, *J. Chem. Phys.*, 1985, **83**, 735.
49 T. Ziegler and A. Rauk, *Theor. Chim. Acta*, 1977, **46**, 1–10.
50 G. te Velde, F. M. Bickelhaupt, E. J. Baerends, C. Fonseca Guerra, S. J. A. van Gisbergen, J. G. Snijders and T. Ziegler, *J. Comput. Chem.*, 2001, **22**, 931–967.
51 E. van Lenthe, E. J. Baerends and J. G. Snijders, *J. Chem. Phys.*, 1994, **101**, 9783.
52 E. R. Johnson, S. Keinan, P. Mori Sánchez, J. Contreras García, A. J. Cohen and W. Yang, *J. Am. Chem. Soc.*, 2010, **132**, 6498–6506.
53 J. Contreras-García, E. R. Johnson, S. Keinan, R. Chaudret, J.-P. Piquemal, D. N. Beratan and W. Yang, *J. Chem. Theory Comput.*, 2011, **7**, 625–632.

